Direct reaction description of sub- and above-barrier fusion of heavy ions

T. Udagawa, B. T. Kim,* and T. Tamura
Department of Physics, University of Texas, Austin, Texas 78712
(Received 26 November 1984)

A new approach to calculation of the fusion cross section σ_F, based on the direct reaction concept, is presented. The method is to define a fusion potential W_F [with $r \leq R_F = r_F(A_1^{1/3} + A_2^{1/3})$] as a part of the imaginary potential of the usual optical model. The σ_F is then obtained as that part, due to only W_F, of the total absorption cross section. It is seen that, if r_F is chosen as 1.40—1.50 fm, the value of σ_F computed as described fits the experimental σ_F very well, in both sub- and above-barrier regions, and for a variety of fusing nuclear pairs A_1 and A_2. In most cases, it is sufficient to consider only the incident (elastic scattering) channel. In a few cases, in which some specific nuclear structure effects are involved, it is found necessary to perform coupled-channel calculations. Then absorption due to other channels is also taken into account explicitly. It is shown that adding these contributions is the key to getting good fits to data, under the above-mentioned special circumstances. A possible relation of what the present approach describes, particularly when it is used in the sub-barrier region, to (spontaneous) fission is also discussed.

I. INTRODUCTION

Fusion of two heavy ions has customarily been described in terms of simple models that use one-dimensional potentials.[1,2] In this model, fusion is assumed to take place if (and only if) the two ions pass through (or go over) the potential barrier. The model is thus often referred to as the barrier penetration model (BPM).

In the sub-barrier regime, the barrier penetrability is calculated first, and is used to deduce the fusion cross section σ_F. In the above-barrier regime, on the other hand, the two ions are considered to fuse, if the potential barrier height, which includes the centrifugal potential, is lower than the value of incident energy $E_{\text{c.m.}}$. The cross section is thus obtained as a sum of contributions from the partial waves that satisfy this criterion.

Experimental evidence shows, however, that the simple BPM has troubles. In the sub-barrier case, the BPM often underestimates[1-9] the measured σ_F. On the other hand, the very simple BPM, mentioned above, overestimates[1,10] the experimental σ_F (particularly for very heavy systems).

In order to remove these troubles, a variety of attempts were made recently.[3-9,11-16] In the sub-barrier region, the approach usually made is to stay with the BPM, but to allow for varying the parameter involved rather freely. This is done with the premise that such variations would take into account the effects of neck formation,[3] or the zero-point oscillation of the nuclear shape.[4,5] Such modifications of the BPM certainly resulted in enhanced sub-barrier fusion cross sections, thus improving the fit to data. In dealing with the effect of the zero-point oscillations, some authors also used the coupled channels (CC) method.[7-9,11-14]

For the above-barrier case, e.g., Swiatecki[15] proposed a model called the extra-push model. It is a two-dimensional potential model in that he added the neck formation degree of freedom to the usual BPM. (He also added a frictional force.) With this model Swiatecki was able to explain the observed reduction of the cross sections. A similar two-dimensional model was developed also by Grègoire *et al.*[16] They used the asymmetry degree of freedom, in place of that of neck formation.

It may be worthwhile to note here that all the above modifications of the simple BPM were made, having in mind their use only in the sub-barrier or in the above-barrier region. It does not seem likely that any of these modifications would remove the troubles in both regions simultaneously.

It may also be remarked that the BPM, including its modifications, often contradicts the fact that sizable amounts of direct reactions are taking place even (somewhat) below the barrier. Also, the real and imaginary potentials (in particular the latter) used in the BPM are normally quite different from those of the usual optical model potentials. This means that, by using the BPM, one normally gives up any hope of fitting even very simple elastic scattering data.

It is our strong belief that it is highly desirable to construct a theory for fusion, which is consistent with the concept of the direct reaction (DR); or at the least with elastic scattering. This is why we proposed recently[17,18] an approach to calculate σ_F, within the framework of the DR theory. (This, in particular, means that we always use optical potentials that fit elastic scattering data.)

The purpose of the present paper is to explain this new approach in detail. As will be seen below, we can describe the sub- and above-barrier fusions (as well as the DR processes) on the same footing.

The basic idea is to define a fusion potential $W_F(r)$, as a part of the imaginary potential $W(r)$ in the usual optical model. We then obtain σ_F as that part, which is due solely to $W_F(r)$, of the total reaction cross section (normally denoted by σ_R). In the simplest case, we consider only elastic scattering, as the DR mode that comes into our description of σ_F. As will be shown below, σ_F is then

written as (a constant times) the expectation value of $W_F(r)$, with respect to the distorted wave in this elastic channel.

We denote the above fusion cross section by $\sigma_{\rm EF}$ (rather than σ_F), to emphasize the fact that it was calculated by using quantities that pertain only to the elastic channel. The EF stands for elastic fusion, and we call $\sigma_{\rm EF}$, somewhat loosely, the *cross section for fusion that takes place in (or proceeds through) the elastic channel.* To describe $\sigma_{\rm EF}$ in this way is very much the same as to call σ_R the total reaction cross section described purely in terms of the optical model. The σ_R is the sum of cross sections of all the reactions, many of them going though complicated steps. Likewise, $\sigma_{\rm EF}$ includes fusion processes that may go first into some other DR channels, and then eventually into the fused state. Nevertheless, we describe $\sigma_{\rm EF}$ entirely within the framework of the optical model.

There are cases in which we find that we cannot fit experimental σ_F simply in terms of $\sigma_{\rm EF}$. These are cases in which a few channels exist, which are coupled to the elastic channel and play some specific role for enhancing σ_F. For such cases, we consider these channels explicitly, by switching our DR description from that of the simple optical model to that of the CC or CRC (coupled-reaction channel) calculations. A new description of σ_F then emerges, and we succeed in regaining the fit to data.

The next section, i.e., Sec. II, is devoted to the presentation of our formalism. In Sec. II A, we explain how to obtain $\sigma_{\rm EF}$, while in Sec. II B, we formulate σ_F for the case in which CC or CRC calculations are needed. In Sec. III A, we compare with data the prediction of $\sigma_{\rm EF}$. As seen, we achieve good fits to data in many cases, covering both sub- and above-barrier regions. In Sec. III B, we attempt, by concentrating our attention on the above-barrier region, to obtain a deeper insight into physics described by our calculations. In Sec. IV, we discuss the cases in which we need to use the formalism of Sec. II B, and show that we can indeed fit nicely some data which we were unable to handle in Sec. III. Section V is devoted to a summary of the present work, and also to a few additional discussions, including a possible relation between the fusion process (as described in our way) and its inverse process, i.e., fission.

II. FORMULATION

A. Elastic fusion

Let us begin by writing the well-known Schrödinger equation for elastic scattering from an optical potential (the standard optical model calculation). It reads

$$(T_a+U_a)\chi_a^{(+)}=E_a\chi_a^{(+)} , \tag{1a}$$

with

$$U_a=-V_a-iW_a . \tag{1b}$$

The subscript a attached to the various quantities that appear in Eq. (1) stands for the elastic channel a, which will be treated as the incident channel, when we consider more complicated direct reactions later on. In Eq. (1b), $-V_a$ and $-W_a$ are, respectively, the real and imaginary parts of the optical potential U_a (for the a channel), and $\chi_a^{(+)}$ is the distorted-wave function.

With Eq. (1), the total reaction cross section σ_R can be written as

$$\sigma_R=(2\pi/\hbar v_a)(\langle\chi_a^{(+)}\,|\,W_a\,|\,\chi_a^{(+)}\rangle/\pi) , \tag{2}$$

v_a being the relative velocity. Noting that $\chi_a^{(+)}$ can be expanded into partial waves as

$$\chi_a^{(+)}=(1/k_ar)\sum_{l_a=0}^{\infty}(2l+1)\chi_{l_a}(r)P_{l_a}(\theta) , \tag{3a}$$

Eq. (2) is rewritten as

$$\sigma_R=(\pi/k_a^2)\sum_{l_a=0}^{\infty}(2l_a+1)T_{l_a}\quad\left[\equiv\sum_{l_a=0}^{\infty}\sigma_R^{(l_a)}\right] , \tag{3b}$$

where k_a is the wave number, while T_{l_a}, the penetration factor, is given as

$$T_{l_a}=(4/\hbar v_a)\int_0^{\infty}|\chi_{l_a}(r)|^2W_a(r)dr . \tag{3c}$$

We are ready to present our very basic idea[17] on how to describe the fusion cross section. It is to consider that only a part $W_{F;a}$ of W_a is responsible for fusion. This means that, corresponding to (2), we write the fusion cross section as

$$\sigma_{\rm EF}=(2\pi/\hbar v_a)(\langle\chi_a^{(+)}\,|\,W_{F;a}\,|\,\chi_a^{(+)}\rangle/\pi) . \tag{4}$$

It is important to note that the $\chi_a^{(+)}$ that appears in (4) is *exactly* the same as is the $\chi_a^{(+)}$ in (2). In other words, in spite of the use of $W_{F;a}$ in (4) the full W_a of (1b) is used in order to generate $\chi_a^{(+)}$ of (4). [Namely, we do not recalculate $\chi_a^{(+)}$ of Eq. (4) by using $W_{F;a}$.] As we stated above, $W_{F;a}$ is taken as a part of W_a. The other part of W_a (i.e., the difference $W_a-W_{F;a}$) may then be considered to describe the absorption due to the direct reactions. This means that, with the $\chi_a^{(+)}$, we can take into account both fusion and direct reaction effects in Eq. (4). We finally note here that we denoted in (4) the fusion cross section by $\sigma_{\rm EF}$, rather than by σ_F, as emphasized in the Introduction.

Before proceeding, we shall go back to Eqs. (1)—(3), and remark that the full imaginary potential W_a can be given a microscopic description in the form[19,20]

$$W_a=-{\rm Im}\left\langle\phi_a\phi_A\left|v_a\frac{1}{E-H+i\epsilon}v_a\right|\phi_a\phi_A\right\rangle . \tag{5}$$

In (5), v_a denotes the exact initial state interaction.[19,20] Once written in the form of (5), W_a can be expressed as a sum of contributions from all the possible reaction products (or reaction channels). [One can easily see this by introducing a complete set of final state wave functions, in order to represent the *exact* Green's function $(E-H+i\epsilon)^{-1}$ that appears in (5).] Suppose that we can calculate the contribution to W_a from all the direct reaction channels, and denote it by $W_{{\rm DR};a}$. Then, the rest, i.e., $W_a-W_{{\rm DR};a}$ is nothing but our $W_{F;a}$. Of course, it is impracticable to obtain $W_{{\rm DR};a}$ from (5), and hence $W_{F;a}$. Nevertheless, Eq. (5) serves to give a formal justification for dividing W_a into parts (this time into two parts).

In this sense, the statement which we made above Eq. (4) that $W_{F;a}$ is a part of W_a is very important. It means that an inequality

$$-W_a(r) \leq -W_{F;a}(r) \ ; \ \text{(all } r\text{)} \tag{6}$$

must be satisfied, because, otherwise, $-W_{\mathrm{DR};a}(r)$ can become positive for some values of r, i.e., it becomes a probability source rather than a sink. This is unphysical.

Within this restriction that $W_{F;a}$ must be a part of W_a, probably the simplest choice we may make in practice would be to set[21]

$$W_{F;a} = \begin{cases} W_a \ , & \text{for } r \leq R_F \\ 0 \ , & \text{for } r > R_F \end{cases} \ , \tag{7a}$$

with

$$R_F = r_F(A_1^{1/3} + A_2^{1/3}) \ . \tag{7b}$$

In practice, we treat r_F as adjustable, for each colliding pair A_1 and A_2 (but keep it independent of the incident energy $E_{\mathrm{c.m.}}$). In this sense, the present theory is a one-parameter theory. We may improve the theory by introducing two parameters, the radius and the diffuseness, for instance. [Keep in mind the restriction of (6).] Such an improvement, however, will not be sought for in the present work. As will be seen below, the one-parameter theory works surprisingly well, with a rather narrow range of the values of r_F; $r_F = 1.4 \sim 1.5$ fm.

Once the above choice of Eq. (7) is made for $W_{F;a}$, we can rewrite Eq. (4) as

$$\sigma_{\mathrm{EF}} = (\pi/k_a^2) \sum_{l_a=0}^{\infty} (2l_a+1) T_{F;l_a} \quad \left[\equiv \sum_{l_a=0}^{\infty} \sigma_{\mathrm{EF}}^{(l_a)} \right] \ , \tag{8a}$$

with

$$T_{F;l_a} = (4/\hbar v_a) \int_0^{R_F} |\chi_{l_a}(r)|^2 W_a(r) dr \ , \tag{8b}$$

which is to be compared with Eq. (3). As seen, Eq. (8b) differs from Eq. (3c), only in that the r integral in the former has an upper limit R_F.

B. Direct-reaction fusion

As will be shown in Sec. III, there are a few cases in which the use of Eq. (4) [or Eq. (8)] with Eq. (7) encounters difficulties in fitting (sub-barrier) fusion data. These are the cases in which there exist a few DR channels, through which specifically a large amount of fusion can take place.

What we intend to do now is to develop a description of the fusion processes, that take place not only in channel a, but also in channels b that are reached via DR processes denoted by $A(a,b)B$. To be more precise, we treat the direct reaction by means of the CC (Ref. 22) or CRC (Ref. 23) method.

The DR processes (that we consider explicitly in the CC or CRC calculations), and the subsequent fusion processes proceeding through these DR channels, are all contained in W_a given by Eq. (5). Let us denote the contribution, to W_a, from these reactions by $W_{D;a}$. We may then write W_a as

$$W_a = W_a' + W_{D;a} \ , \tag{9a}$$

where W_a' describes the rest of the contributions to W_a, thus serving as the (usual) imaginary potential to be used in the CC calculations. We call the optical potential to be used in the CC calculation the *CC potential,* and distinguish it from the *elastic potential* of Eq. (1) (used in the simple optical model calculation). We denote this CC potential by U_a'. The W_a' is then nothing but (the negative of) the imaginary part of U_a'. Now, $W_{D;a}$ may be cast into a form similar to Eq. (5) as

$$W_{D;a} = -\mathrm{Im}\langle \phi_a \phi_A \mid U_D^+ G_D^{(+)} U_D \mid \phi_a \phi_A \rangle \ , \tag{9b}$$

where $G_D^{(+)}$ is the Green's function corresponding to the DR Hamiltonian H_D that is constructed for the CC or CRC calculations at hand.

The fusion part $W_{F;a}'$ of W_a' may be singled out in exactly the same way as done [in Eq. (7)] for W_a. In order to single out the fusion part from $W_{D;a}$, we may now use the method developed earlier to calculate the breakup-fusion cross section.[24] In fact, all we need to do is to use an identity given as

$$G_D^{(+)} = \Omega_b^{(-)} g_b^{(+)} \Omega_b^{(-)+} - G_D^{(+)} U_D^+ G_D^{(+)+} \ . \tag{10}$$

Equation (10) is obtained as a limit to the two-body channel of the more general relation valid for the three-body channel, given in Ref. 24.

In Eq. (10), $\Omega_b^{(-)}$ and $g_b^{(+)}$ are, respectively, the wave operator and the plane wave Green's function in the b channel. The operator $\Omega_b^{(-)}$ produces the coupled channel wave function when it is operated upon the plane wave function, and is defined as

$$\Omega_b^{(-)} = 1 + G_D^{(+)+} U_D^+ \ . \tag{11}$$

By inserting (10) into (9b), we see that the latter is rewritten as

$$W_{D;a} = -\mathrm{Im}(\langle \phi_a \phi_A \mid U_a^+ \Omega_b^{(-)} g_b \Omega_b^{(-)+} U_a \mid \phi_a \phi_A \rangle + \langle \phi_a \phi_A \mid U_a^+ G_D^{(+)} W_b' G_D^{(+)} U_a \mid \phi_a \phi_A \rangle) \ . \tag{12}$$

In Eq. (12), it is clear that the first term describes the contributions to $W_{D;a}$ from the direct reactions that end up in the channel(s) b. On the other hand, the second term originates from the absorption that takes place in these b channels. The contribution to σ_F from the b channels may then be obtained from the second term of (12), in which W_b' is replaced by $W_{F;b}'$, e.g., by using Eq. (7) again. (Here we assume that the interactions that couple channels are purely real. The final expression [Eq. (17)] given below is, however, valid even if the coupling interactions are complex.)

Summarizing, the total fusion cross section can now be written as

$$\sigma_F = \sigma_{\mathrm{EF}}' + \sigma_{\mathrm{DRF}} \ , \tag{13}$$

where σ_{EF}' and σ_{DRF} are the contributions to σ_F from the fusion taking place in the elastic and DR channels, respectively. They are given explicitly as

$$\sigma_{\mathrm{EF}}' = (2\pi/\hbar v_a)(\langle \chi_a^{(+)} \mid W_{F;a}' \mid \chi_a^{(+)} \rangle / \pi) \tag{14a}$$

and

$$\sigma_{\rm DRF}=(2\pi\hbar v_a)(\langle\Phi_b^{(+)}\mid W'_{F;b}\mid\Phi_b^{(+)}\rangle/\pi)\ . \tag{14b}$$

In Eq. (14) $\Phi_b^{(+)}$ is the relative wave function in the b channel, and is given by

$$\Phi_b^{(+)}=(\phi_b\phi_B\mid G_D^{(+)}U_a\mid\chi_a^{(+)}\phi_a\phi_A\rangle\ . \tag{15}$$

In terms of $\Phi_b^{(+)}$ the total CC wave function $\Psi_a^{(+)}$ can be written as

$$\Psi_a^{(+)}=\chi_a^{(+)}\phi_a\phi_A+\sum_b\Phi_b^{(+)}\phi_b\phi_B\ . \tag{16}$$

Noting that $W_{F;c}$ ($c=a$ and b) has no nondiagonal element, it is possible to combine the two terms in Eq. (13) to produce a more compact form,

$$\sigma_F=(2\pi/\hbar v_a)(\langle\Psi_a^{(+)}\mid W'_F\mid\Psi_a^{(+)}\rangle/\pi)\ , \tag{17}$$

where W'_F is an operator whose projection onto the c channel is nothing but $W'_{F;c}$ ($c=a$, b, etc.).

From the derivation given above, it is clear that the fusion cross section formulas given by Eqs. (4) and (17) are equivalent, at least in principle. In Eq. (17), the fusion processes proceeding via specific direct reaction channels are treated explicitly, while in Eq. (4), they were included only implicitly in $W_{F;a}$. In practice, the results that are obtained from Eqs. (4) and (17) are different, unless we, e.g., make the potential $W_{F;a}$ in (4) nonlocal, so as to take into account effects of specific channels.

III. ELASTIC FUSION CROSS SECTIONS

In subsection A, we present the results of numerical calculations of $\sigma_{\rm EF}$, made based on Eq. (4), and compare them with experiment. As seen, the calculations cover both the sub- and above-barrier regions. In subsection B, we then discuss some specific features of $\sigma_{\rm EF}$ seen in particular in the above-barrier region.

A. Results of numerical calculations and comparison with experiment

So far we have performed calculations for 14 systems, as listed in Table I. In this table, we also present the optical model parameters for each system. These parameters were taken from the literature,[7,25–28] except those for the Ni + Ni and Br + A (A=Zr, Mo, and Ru) systems. For the Ni + Ni system, we extracted parameters by analyzing data for elastic scattering of the ^{60}Ni+^{58}Ni system taken at $E_{\rm c.m.}=112.1$ MeV.[29] [To be precise, a set of optical parameters for the ^{60}Ni+^{60}Ni system, extracted from a CC analysis, was given in Ref. 29. However, the use of this set, which used a rather small radius parameter, 1.2 fm, resulted in a poor fit to the fusion data. We thus obtained new parameters by performing an (uncoupled) optical model analysis, fitting, however, only the large angle data. For this reanalysis, we used data for ^{60}Ni+^{58}Ni, instead of ^{60}Ni+^{60}Ni, in order to avoid the necessary symmetrization of the transition amplitude when the latter system is considered.] As for the Br + A system (or for any nearby system), neither optical potential nor elastic scattering data are available. We thus simply used for these systems the parameters of the Ca + Ca system.

For all the systems, the calculations were made with an energy-independent optical potential, as shown in Table I, as well as the energy-independent r_F also listed in Table I. An exception was the ^{16}O+^{208}Pb system in which energy dependent optical parameters were available.[25] We thus carried out calculations for this system by using these energy-dependent potential parameters, yet with fixed r_F. We also note that the radius parameters of the imaginary potential for the Ni + Sn system were modified from the value 1.26 fm, given in Ref. 28, to 1.35 fm. Such a modification did not alter the fit to the elastic scattering data, but improved noticeably the fit to the fusion data. (For this reason, we may say that to fit σ_F data is a better way

TABLE I. Optical potential parameters used in the calculations.

Systems	V (MeV)	W (MeV)	r_0 (fm)	r_I (fm)	r_c (fm)	a_R (fm)	a_I (fm)	$r_{\rm F}$ (fm)	References Expt.	References OMP	V_B (MeV)
^{16}O+^{148}Sm	20.0	20.0	1.34	1.34	1.25	0.57	0.36	1.46	6	7	59.5
^{16}O+^{154}Sm	20.0	20.0	1.34	1.34	1.25	0.57	0.36	1.46	6	7	59.1
^{16}O+^{208}Pb	100.0	22.0	1.25	1.25	1.25	0.50	0.50	1.45	25	25	73.8
^{40}Ar+^{122}Sn	41.8	8.0	1.25	1.34	1.25	0.51	0.39	1.50	5	26	108
^{40}Ca+^{40}Ca	35.0	12.13	1.35	1.35	1.35	0.43	0.43	1.46	30,31	27	53.2
^{40}Ca+^{44}Ca	35.0	12.13	1.35	1.35	1.35	0.43	0.43	1.46	31	27	52.4
^{58}Ni+^{58}Ni	40.0	15.0	1.25[a]	1.25[a]	1.25[a]	0.55	0.55	1.45	9	29	95.6
^{58}Ni+^{64}Ni	40.0	15.0	1.25[a]	1.25[a]	1.25[a]	0.55	0.55	1.45	9	29	94.1
^{58}Ni+^{124}Sn	58.1	62.9	1.26	1.35[b]	1.26	0.294	0.294	1.42	28	28	165
^{64}Ni+^{118}Sn	58.1	62.9	1.26	1.40[b]	1.26	0.294	0.294	1.46	28	28	164
^{81}Br+^{90}Zr	35.0	12.13	1.35	1.35	1.35	0.43	0.43	1.41	30	27	154
^{81}Br+^{94}Zr	35.0	12.13	1.35	1.35	1.35	0.43	0.43	1.41	30	27	153
^{81}Br+^{94}Mo	35.0	12.13	1.35	1.35	1.35	0.43	0.43	1.41	30	27	161
^{81}Br+^{104}Ru	35.0	12.13	1.35	1.35	1.35	0.43	0.43	1.41	30	27	166

[a]The original value is 1.20.
[b]The original value is 1.26.

to fix the imaginary part of the optical potential than to fit the elastic scattering cross section.)

In Figs. 1—7, the calculated σ_{EF} are presented as functions of $E_{c.m.}$, and are compared with the experimental data. (References 5, 6, 9, 28, and 30—32, from which the data were taken, are all listed in Table I.) As seen, the overall fit to the data is very good.

The two theoretical results, shown in Fig. 2 for $^{16}O+^{208}Pb$, by the dotted and full lines, respectively, are those obtained by using the energy independent and energy dependent parameters.[25] (The former used the parameters given[25] at $E_{c.m.}=75$ MeV.) Comparison of these two results gives an idea on how the calculation depends on the potential parameters that are used. As seen in Fig. 2, the difference between them is not very significant, although it is worthwhile to emphasize that the solid line appears below the dotted line at the higher $E_{c.m.}$.

Two different theoretical curves are also shown in Fig. 3 by the full and broken lines. They are, respectively, the results with the present theory and BPM.[5] The latter curve was presented to exemplify the rapid decrease of the sub-barrier cross section, when the BPM is used, as remarked in the Introduction.

In spite of the good overall fit to the data, achieved in Figs. 1—7, one sees notable discrepancies in a few cases, such as the $^{16}O+^{154}Sm$, $^{40}Ca+^{44}Ca$, and $^{58}Ni+^{64}Ni$ systems. These are, however, the cases in which specific channels play important roles, and thus are to be analyzed by using the formalism of Sec. II B rather than that of Sec. II A. We shall discuss these special cases in Sec. IV.

We also note that the large discrepancy seen in Fig. 7 should not be taken as an indication of a trouble of our

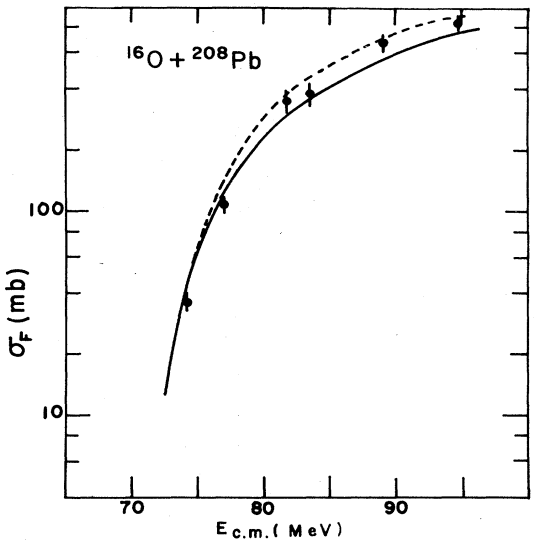

FIG. 2. Comparison of calculated (σ_{EF}) and experimental fusion cross sections for the $^{16}O+^{208}Pb$ system. The full and dotted curves shown are σ_{EF} calculated by using the energy dependent and independent optical parameters.

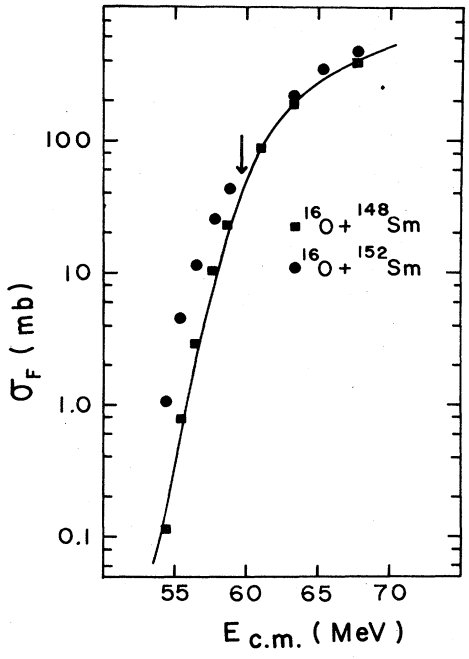

FIG. 1. Comparison of calculated (σ_{EF}) and experimental fusion cross sections for the $^{16}O+^{148,152}Sm$ systems. Since the calculated σ_{EF} of the $^{16}O+^{148}Sm$ and $^{16}O+^{152}Sm$ systems are almost identical, we plotted here only σ_{EF} for the $^{16}O+^{148}Sm$ system. The arrow indicates the position V_B, of the s-wave barrier top for the $^{16}O+^{148}Sm$ system.

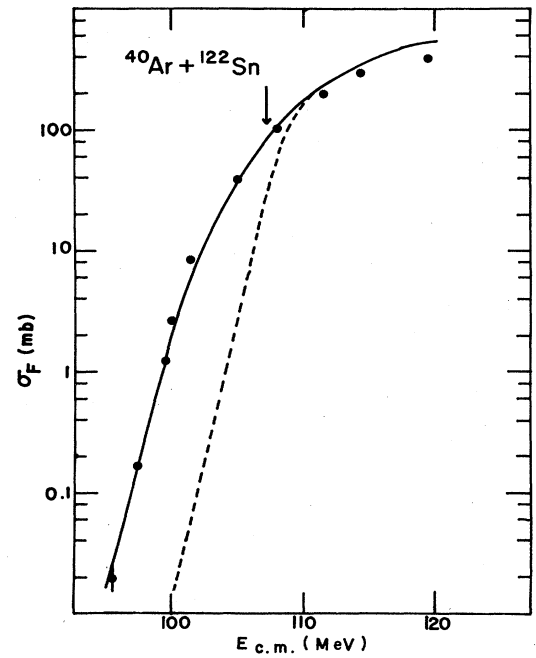

FIG. 3. Comparison of calculated (σ_{EF}) and experimental fusion cross sections for the $^{40}Ar+^{122}Sn$ system. The full and dashed curves are, respectively, the fusion cross sections calculated by the present theory and BPM. The arrow indicates the position V_B of the barrier top.

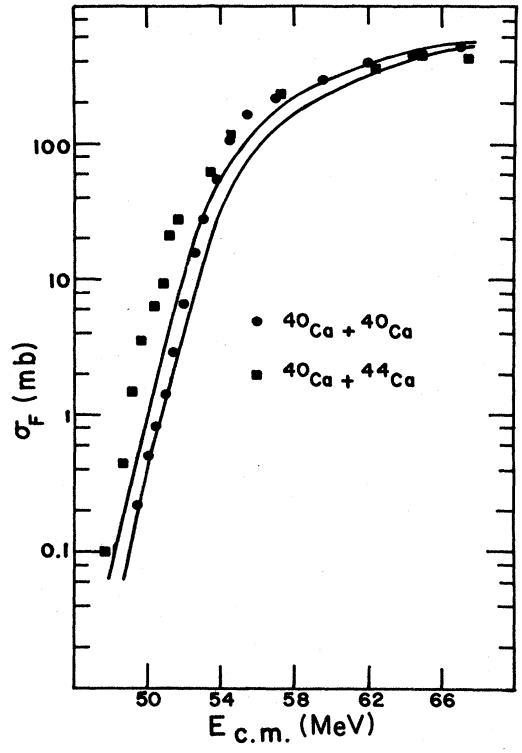

FIG. 4. Comparison of calculated (σ_{EF}) and experimental fusion cross sections for the $^{40}Ca+^{40,44}Ca$ systems.

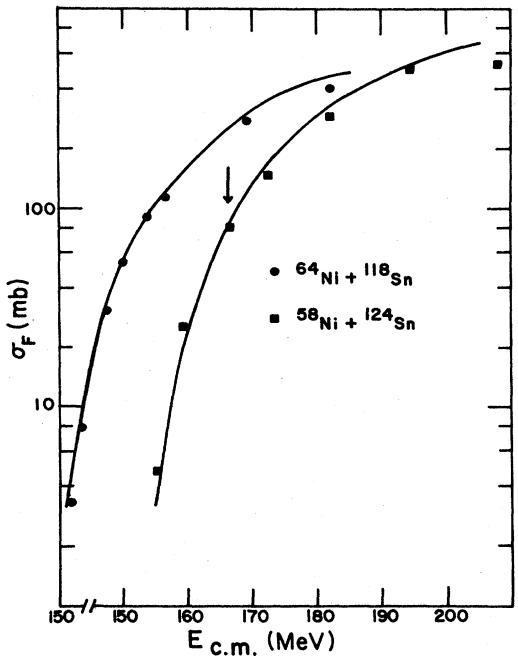

FIG. 6. Comparison of calculated (σ_{EF}) and experimental fusion cross sections of the $^{64}Ni+^{118,124}Sn$ systems. The arrow indicates the position V_B of the barrier top for the $^{58}Ni+^{124}Sn$ system.

approach. The data plotted include only the evaporation residue cross sections. For the systems considered in Fig. 7, however, the so-called fusion-fission cross sections are expected to be rather large, particularly for larger $E_{c.m.}$ (as suggested by the work of Henning *et al.*[28]). One sees that our σ_{EF} in Fig. 7 consistently overestimates the experimental σ_F. We hope that this gap will be filled by a further measurement of the fusion-fission cross sections.

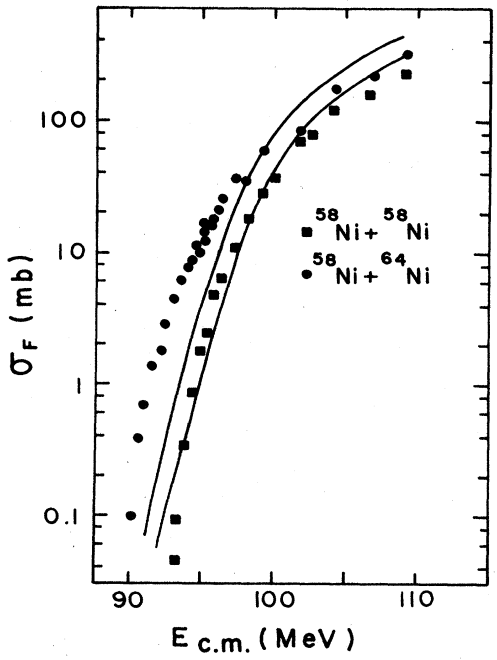

FIG. 5. Comparison of calculated (σ_{EF}) and experimental fusion cross sections for the $^{58}Ni+^{58,64}Ni$ systems.

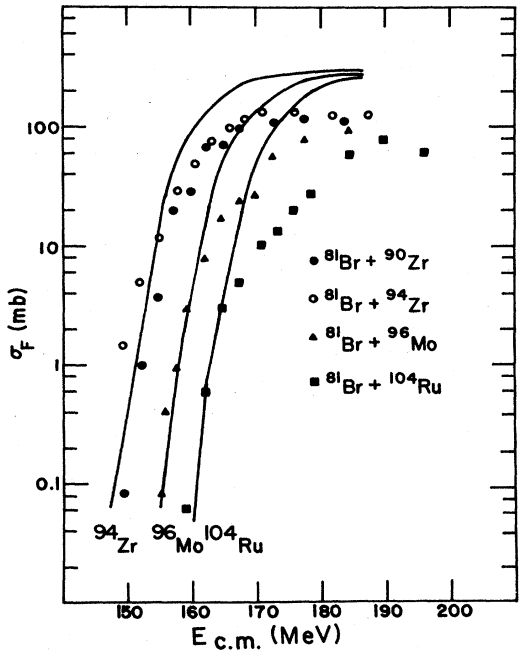

FIG. 7. Comparison of calculated (σ_{EF}) and experimental fusion cross sections of the $^{81}Br+^{92,94}Zr$, $^{81}Br+^{96}Mo$, and $^{81}Br+^{104}Ru$ systems.

B. σ_{EF} in the above barrier

As shown above, the calculated σ_{EF} fit the experimental σ_F rather well (excluding the special cases discussed towards the end of the last subsection). Note that the barrier height V_B is indicated by arrows for three systems; $^{16}O+^{148}Sm$, $^{40}Ar+^{122}Sn$, and $^{58}Ni+^{124}Sn$ (see Figs. 1, 3, and 6, respectively). These are the cases in which our σ_{EF} fit the data almost perfectly, and the positions of the arrows show that the fits were achieved covering both the sub- and above-barrier regions. In other words, we have succeeded in explaining the sub- and above-barrier fusion cross sections on an equal footing. (If $E_{c.m.}$ is increased beyond the energies considered in Figs. 1—7, the experimental σ_F begins to saturate or decrease. We do not consider such a high $E_{c.m.}$ regime in the calculations made in the present paper, but a qualitative discussion of it will be given in Sec. IV.)

As is well known, in the above-barrier region, the experimental σ_F is essentially proportional to $1/E_{c.m.}$. This means more quantitatively that σ_F can be well represented by a linear function written as

$$\sigma_F=\pi R_c^2(1-V_B/E_{c.m.}) . \tag{18}$$

Here R_c and V_B are arbitrary parameters, whose values may be fixed by fitting the data.

Theoretically, the observed linear dependence of σ_F has been understood in terms of a simple one-dimensional potential model.[1] In such a model it is assumed that only the partial waves, up to an orbital angular momentum l_B whose potential barrier height equals $E_{c.m.}$, contribute to the fusion; a sharp cutoff model. The fusion cross section is then given by

$$\sigma_F=(\pi/k_a^2)(l_B)^2 . \tag{19}$$

Further, use is made of a relation that

$$l_B=R_B[\hbar^2(E_{c.m.}-V_B)/2\mu]^{1/2} , \tag{20}$$

V_B being the height of the s-wave barrier top that is located at $r=R_B$. If (20) is inserted into (19), Eq. (18) follows.

It is important to note, however, that the cross section formula (18), as derived in the way as described just above, requires that

$$R_c=R_B . \tag{21}$$

This means that the parameters R_c and V_B in Eq. (18) are not independent of each other, but are mutually related. We may call Eq. (21) a classical condition, since it resulted from the use of the classical (or semiclassical) relations (19) and (20). Experimentally, this condition is rather well satisfied in fusion of relatively light systems [with a small effective fissility parameter $X_{eff}=(Z^2/A)_{eff}$]. Recent measurements,[10] however, revealed that the condition (21) is not satisfied in fusion of very heavy systems with large X_{eff} values. (The parameter R_c gets much smaller than R_B as X_{eff} gets larger.)

In Fig. 8, the experimental σ_F and calculated σ_{EF} are plotted on a linear scale, against $1/E_{c.m.}$, for three selected cases, the $^{16}O+^{148}Sm$, $^{40}Ar+^{122}Sn$, and $^{58}Ni+^{124}Sn$ systems. As seen, they are all fitted very well by straight lines. (Comparison of the solid and dashed straight lines in Fig. 8 shows that we are slightly overestimating the cross sections at higher $E_{c.m.}$. The result of Fig. 2 shows that the use of the energy dependent optical potential does help in removing this undesired feature.)

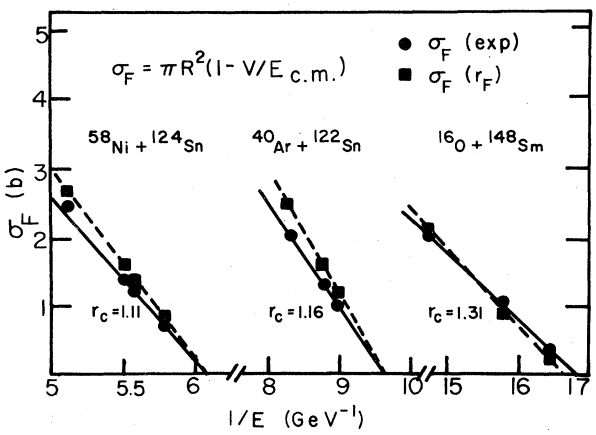

FIG. 8. Linear plot of the calculated and experimental cross sections against $1/E_{c.m.}$, and extraction of R_c and V_B parameters of Eq. (18).

From the straight lines shown in Fig. 8, we can determine the values of V_B and r_c (defined as R_c divided by $A_1^{1/3}+A_2^{1/3}$). They are $V_B=59$, 104, and 164 MeV, and $r_c=1.31$, 1.16, and 1.11 fm, respectively, for the above three systems. With the optical parameters we use, the top of the (s wave) barrier appears at $R_B=11.3$, 11.4, and 11.9 fm, which means that the reduced r_B values are 1.44, 1.36, and 1.34 fm, respectively. (The height V_B of the barrier at these R_B agrees very well with the V_B values deduced above, as was expected.)

The value of r_c is fairly close to r_B in the case of the $^{16}O+^{148}Sm$ system (that has the smallest X_{eff}), but is much smaller than r_B in other systems with larger X_{eff}. In order to show this more clearly, we plot in Fig. 9 the r_c and r_B values as functions of X_{eff}, where we also show the values of r_F. As seen, r_B and r_F stay almost constant, while r_c decreases rather fast as X_{eff} increases. This means that the classical condition, Eq. (21), cannot be maintained for the case with a large X_{eff}. Compared with this, our theory explains the difference between r_c and r_B

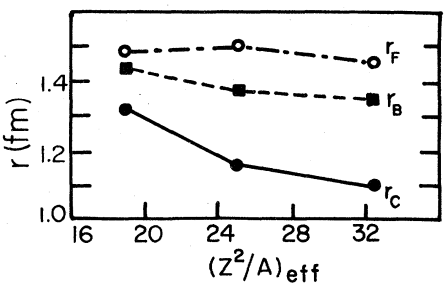

FIG. 9. Comparison of the r_c, r_B, and r_F parameters for three systems in Fig. 8.

more or less automatically. We shall now show that this success is due to our use of the realistic optical potential (and possibly to a reasonable choice of R_F).

As the first step of doing this, we plot in Fig. 10 the partial cross sections $\sigma_R^{(l)}$ and $\sigma_F^{(l)}$, which are defined, respectively, in (3b) and (8a). (The calculation was done for the ^{58}Ni+^{124}Sn system at $E_{\text{c.m.}}=180$ MeV. Therefore, we are above V_B by about 16 MeV.) Note that (the calculated) $\sigma_R^{(l)}$ is essentially linear for l up to $l=l_B=65$ (which is marked by a vertical line in Fig. 10), and have the value that agrees with the (semi-) classical value $(2l+1)\pi/k^2$. We also draw a vertical line in Fig. 10 marked l_c (with $l_c=58$), and the experimental σ_F agrees with the area of the triangle defined by the $\sigma_R^{(l)}$ and the l_c lines. The fact that one has to use an l_c which is smaller than l_B, is, of course, the same as the requirement that one has to take R_c smaller than R_B.

The situation described in our way is quite different. Our partial $\sigma_F^{(l)}$ is shown in Fig. 10 by a dashed line, and the area under this line again agrees with the experimental σ_F. A remarkable feature is that $\sigma_F^{(l)}\neq 0$ for $l\gtrsim l_B$, and that we have $\sigma_F^{(l)}\simeq\sigma_R^{(l)}/2$, for $l\lesssim l_B$. These features, in particular the latter, result from our use of the R_F radius. In our description, about half of the total $\sigma_R^{(l)}$ (for lower l) is due to the DR, and the other half to fusion.

With the purpose of seeing still more closely the origin of the behavior of $\sigma_F^{(l)}$ shown in Fig. 10, we plotted in Fig. 11 the intensity of the absorption $A(r)\equiv|\chi_{l_a}(r)|^2 W_a(r)$, i.e., the integrand of the integral that appears in (3c) and (8b). This is done for the ^{58}Ni+^{124}Sn system (with $E_{\text{c.m.}}=180$ MeV), i.e., the same case considered in Fig. 10, and also for the ^{16}O+^{148}Sm system (with $E_{\text{c.m.}}=64$ MeV). The latter has a much smaller fissility than does the former, and to compare these two cases is very interesting. (Note that the above two cases share the same value of $E_{\text{c.m.}}/V_B=1.09$.)

As seen in Fig. 11(a), the $A(r)$ for the ^{58}Ni+^{124}Sn case is rather narrowly and symmetrically distributed around a radius, whose value is very close to R_F. (This is the case for all the l, ranging from 0 to 60.) It is thus very easy to see (as in Fig. 10) how $\sigma_F^{(l)}=\sigma_R^{(l)}/2$ resulted. [For higher l, the center of $A(r)$ moves to larger r, making $\sigma_F^{(l)}\ll\sigma_R^{(l)}$.]

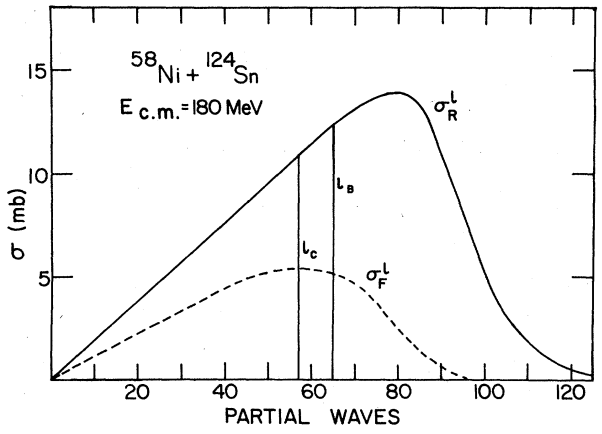

FIG. 10. Partial wave contributions to σ_R and σ_{EF}.

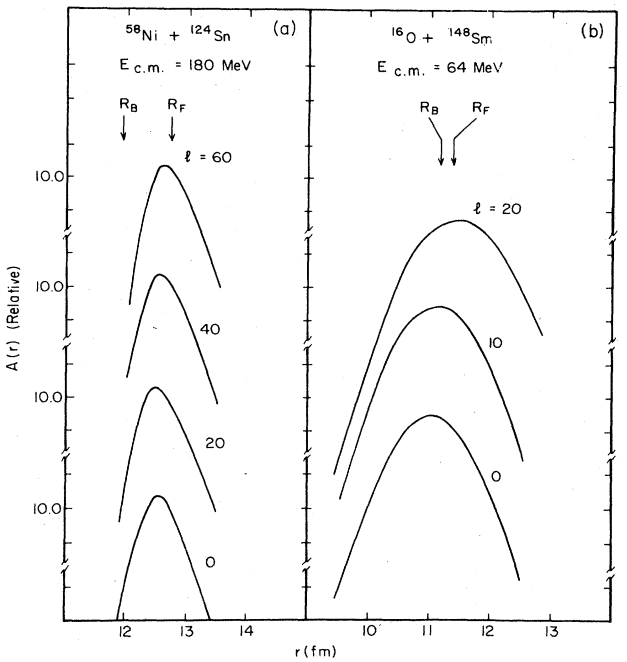

FIG. 11. Radial dependence of the integrands $A(r)$ for several values of the angular momenta l, for the ^{58}Ni+^{124}Sn and ^{16}O+^{148}Sm systems.

The behavior of $A(r)$ for ^{16}O+^{148}Sm seen in Fig. 11(b) is rather different. It now has a much broader structure, and the peak position moves to larger r, as l is increased. At $l=0$, most of the $A(r)$ lies to the left of $r=R_F$, which makes $\sigma_F^{(0)}\simeq\sigma_R^{(0)}$, a fact which explains why $r_c\simeq r_B$ in this system that has a rather small X_{eff}.

It is not difficult to see why $A(r)$ behaves so differently in the two cases. The difference is due to the difference in the strength of the absorption. Note that the (local) mean free path $\lambda(r)$ for the absorption is roughly proportional to $[W(r)\mu]^{1/2}$, where μ is the reduced mass. In the case of ^{58}Ni+^{124}Sn, $\lambda(r)$ is as small as 0.2 fm, in the neighborhood of $r=R_F$. Thus the distorted wave $\chi_{l_a}(r)$ cannot survive, much inside of R_F. The system ^{16}O+^{148}Sm is, however, much less absorptive. Thus the lower partial waves can penetrate deep into the internal region.

Our approach, explained above, which results in $r_c<r_B$ automatically, is quite different from that of the extra-push model of Swiatecki.[15] The $\sigma_F^{(l)}$ predicted by the Swiatecki model equals that of the sharp cutoff model with $l_{\max}=l_c$, the switch of l_B to l_c being explained in terms of the extra-push energy. Thus, his model resorts to the triangle in Fig. 10, and thus has the l distributions of $\sigma_F^{(l)}$ quite different from ours. The differences between these models, may, however, be studied experimentally, by observing, e.g., the (decay) γ-ray multiplicities (from the evaporation residues), or the angular distributions of the fission products. Evidence seen so far in systems with relatively small X_{eff} seems to favor a smooth $\sigma_F^{(l)}$ with a long tail,[25,33] as in our theory.

Concerning the DR contributions to σ_R, it may be worthwhile to refer to a recent experiment performed by Rehm *et al.*[34] They measured total DR cross sections (σ_{DR}) for ^{35}Cl, ^{50}Ti, and ^{58}Ni bombarding ^{208}Pb, and found that $\sigma_{DR}/\sigma_R \simeq 0.15$ in the case of the relatively light ^{35}Cl projectile, but $\sigma_{DR}/\sigma_R \simeq 0.7$ with heavier ^{50}Ti and ^{58}Ni projectiles. These results can be taken as evidence that clearly supports the prediction we have made and presented above.

IV. COUPLED-CHANNEL CALCULATIONS

In Sec. III, we saw that the experimental sub-barrier fusion cross section for the ^{40}Ca+^{44}Ca, ^{58}Ni+^{64}Ni, and ^{16}O+^{152}Sm systems could not be explained satisfactorily in terms of simple σ_{EF} calculations. And we remarked that these systems involve specific channels to be considered explicitly. Actually, the first two of the above systems have positive Q values for some two nucleon transfer reactions (thus differing significantly from their neighboring systems). The ^{16}O+^{152}Sm system, on the other hand, is characterized by the fact that it contains a deformed target. We have given a formula in Sec. II B, to be used for these specific cases. In the present section, we report on calculations done by using this formula.

A. The ^{16}O+^{148,152}Sm systems

Although we found in Fig. 1 that σ_{EF} fits rather well the ^{16}O+^{148}Sm data, we have performed CC calculations for both the ^{16}O+^{148}Sm and ^{16}O+^{152}Sm cases. In doing this, we used for ^{16}O+^{148}Sm the optical parameters listed in Table I, while for ^{16}O+^{152}Sm, we used those fixed earlier by Kim[35] (in his calculations to fit the inelastic scattering data). Note that we expect that the CC effect is rather weak for the ^{16}O+^{148}Sm system. Note also that the inelastic cross section to the 4^+ state is at least one order of magnitude smaller than that to the 2^+ state, even for the case of ^{16}O+^{152}Sm. We thus have considered only the 0^+-2^+ coupling. The deformation parameters were taken from Refs. 7 and 35, respectively, for the ^{16}O+^{148}Sm and ^{16}O+^{152}Sm system.

The obtained σ_F are presented by solid lines in Fig. 12, and it is seen that good fits to data were obtained for both systems. The values of r_F taken were 1.47 and 1.55 fm for the ^{16}O+^{148}Sm and ^{16}O+^{152}Sm systems, respectively. The value for the ^{16}O+^{148}Sm system is the same as the r_F value given in Table I. The value (1.55 fm) of the ^{16}O+^{152}Sm system is, however, somewhat larger than the value given in Table I. This may be due to the rather large imaginary radius parameter (1.40 fm) of Kim's potential of Ref. 35. In Fig. 12, the elastic channel contribution, σ'_{EF}, is also shown by dotted lines, and the difference between this and σ_F, is the contribution from the 2^+ channel, i.e., σ_{DRF}. As expected, σ_{DRF} is seen to be more conspicuous in ^{16}O+^{152}Sm than in ^{16}O+^{148}Sm, particularly for lower $E_{c.m.}$. The total reaction cross section σ_R (seen in the elastic channel) minus the inelastic cross section, i.e., $\sigma_R - \sigma_{2^+}$, is also shown in Fig. 12. This $\sigma_R - \sigma_{2^+}$ (which is larger than the experimental σ_F) is essentially the same as what Stockstad and Gross[7] took as σ_F. In other words, our work differs from theirs only by the introduction of R_F to obtain σ_F.

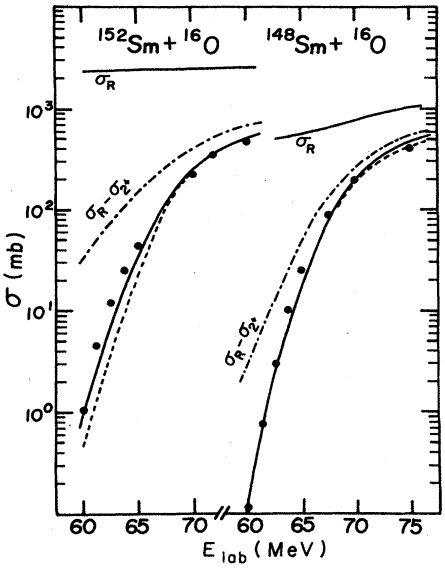

FIG. 12. Comparison of calculated and experimental fusion cross sections for the ^{16}O+^{148,152}Sm systems. The full and dotted curves are $\sigma'_{EF}+\sigma_{DRF}$ and σ'_{EF} only, respectively. See the text for the $\sigma_R - \sigma_{2^+}$ curves.

B. The ^{58}Ni+^{58,64}Ni systems

In our previous study[17] (which was the first application of our method that used R_F), the calculations were made by taking the ^{58}Ni(^{58}Ni,^{56}Ni)^{60}Ni and ^{64}Ni(^{58}Ni, ^{60}Ni)^{62}Ni reactions,[9] which had $Q=-2.1$ and 3.9 MeV, respectively, for the ground-state to ground-state transitions. The spectroscopic amplitudes we used were $A=7.0$ and 8.6, respectively. Actually, these values were chosen so that we could fit the overall magnitude of the observed fusion cross sections. They are somewhat larger than what are calculated (with a reasonable model) for the above ground-state to ground-state transition. We argued in Ref. 17 that the use of these large A values was justified, because, e.g., in the case of the ^{58}Ni+^{64}Ni system, there were several transitions having positive Q values, other than the above ground-state to ground-state transition, which we did not take into account explicitly in the calculation. Also, the calculations of Ref. 17 were made by using DWBA. In this subsection, we report on our new calculations that utilized the CRC method.[23]

It is too laborious to carry out CRC calculations by including all the possible transitions explicitly, and thus we have resorted to the following simplifying treatment. By taking the ^{64}Ni+^{58}Ni system as an example, we assumed that there were three 0^+ transitions, each carrying $\frac{1}{3}$ of the transition strength $|A^2|=74$ (of Ref. 17). We also assumed that these three transitions had Q values of 3.9, 2.5, and 2.5 MeV, respectively. The second of them approximately represents the transitions that lead to the first excited 2^+ states of the final ions, while the third represents the formation of the ^{56}Fe+^{66}Zn system in its

lowest state. We thus expect that our calculation remains fairly realistic. Note, however, that the calculated results do not differ very much from those obtained by considering only one (ground-state to ground-state) transition that carries all the strength. We therefore did the calculation for the ^{58}Ni+^{58}Ni system by considering only one transition, i.e., the ground-state to ground-state transition.

We first used optical parameters given in Table I. However, we found that the CRC calculations modified the elastic scattering cross sections significantly. We thus readjusted some of the parameters, so that the correct elastic scattering cross section was regained as much as possible. (Note the difference between W_a and W_a', discussed in Sec. II B.) We carried out this readjustment at $E_{\text{c.m.}}=95$ MeV. We found that the changes of the r_0 from 1.25 to 1.29 fm and W from 15 and 13.5 MeV achieved the recovery for the ^{58}Ni+^{64}Ni system. The new r_0 and W for the (^{58}Ni+^{58}Ni) system were 1.20 fm and 13.5 MeV, respectively.

It is interesting to stress that we needed to increase r_0 for the ^{58}Ni+^{64}Ni system, and decrease it for the ^{58}Ni+^{58}Ni system. This means that, in the former, the CRC effectively produced a repulsion in the elastic scattering, while for the latter system, it produced an attraction. The origin of these opposing effects may be due to the opposite signs of the Q values in the transitions involved in the two systems, and may be understood on the basis of the argument given recently by Dasso *et al.*[12]

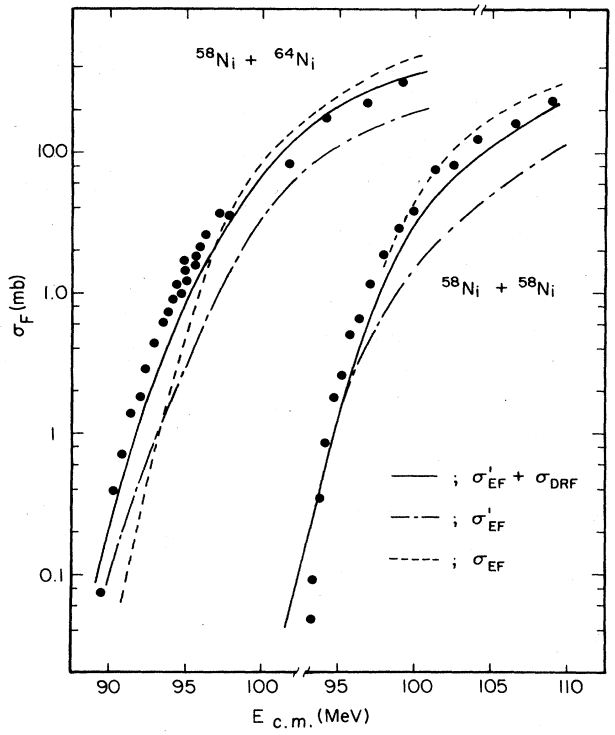

FIG. 13. Comparison of calculated and experimental fusion cross sections for the ^{58}Ni+^{58,64}Ni systems. The full, dashed, and dotted curves are the calculated $\sigma'_{\text{EF}}+\sigma_{\text{DRF}}$, σ'_{EF} only, and σ_{EF}, respectively.

The required decrease of the imaginary potential (by 10%) was more or less as expected.[22]

The calculations were performed by using the same form factors as used in Ref. 17. The results thus obtained are shown by solid lines in Fig. 13. As seen, the calculated σ_F now fits the data very nicely for both systems. The values of r_F used were the same as in Sec. III.

We also show in Fig. 13 the calculated σ'_{EF} and σ_{EF} by dashed and dotted lines, respectively. (The dotted lines are nothing but the full lines shown in Fig. 4.) The difference between the full and dashed lines represents σ_{DRF}. As seen, σ_{DRF} is significant for the ^{58}Ni+^{64}Ni system, particularly for the lower $E_{\text{c.m.}}$. However, it is not very important for the ^{58}Ni+^{58}Ni system as expected.

It should be remarked that for the ^{58}Ni+^{58}Ni system the sum of $\sigma'_{\text{EF}}+\sigma_{\text{DRF}}$ (full line) is roughly equal to σ_{EF} (dotted line). Therefore the equivalence between the two calculated cross sections, discussed in Sec. II B, is fulfilled in this system. This is not the case, however, for the ^{58}Ni+^{64}Ni system. To perform explicit CRC calculations, as done here, is thus vitally needed for this system.[36]

V. CONCLUDING REMARKS

A very simple method to calculate the fusion cross section has been proposed, which can be handled entirely within the framework of the direct reaction theory. The essence of the method is to define a fusion potential $W_F(r)$ as an inner part of the (full) imaginary part of the optical potential $W(r)$ of the optical model. In practice, we introduce a radius parameter, called R_F, so that the $r \leq R_F$ part of $W(r)$ is nothing but $W_F(r)$. The elastic fusion cross section σ_{EF} is expressed as an expectation value of $W_F(r)$ with respect to the distorted wave function in the elastic channel. We found that this simple-minded σ_{EF} fits a number of fusion data very nicely. For the cases in which the simple σ_{EF} was found insufficient, due to the presence of a few specific direct reaction channels that are strongly coupled, we extended the calculations by using the CC or CRC method, and found that good fits to data were recovered.

In cases in which σ_{EF} fit nicely the sub-barrier fusion data, we found that the method worked equally well for the above-barrier fusion data. In other words, we were able to describe the sub- and above-barrier fusion on an equal footing. Note that R_F was kept fixed independent of the energy $E_{\text{c.m.}}$, once the system, i.e., the colliding (fusing) pair A_1 and A_2, was chosen. We also found that $r_F=R_F/(A_1^{1/3}+A_2^{1/3})$, needed to fit the data, was essentially the same ($r_F\simeq 1.45$ fm), for all the systems considered.

Even in cases in which the CC or CRC treatment was necessary, we found that such a need was the case only in the sub-barrier (and slightly above the barrier) region. At higher $E_{\text{c.m.}}$, the fusion cross sections calculated with these complicated methods tended to coincide (approximately) with σ_{EF}.

One of the important consequences in the present analysis is the fact that our r_F ($\simeq 1.45$ fm) was rather large, making $R_F > R_B$, where R_B is the radius at which the s-wave barrier peaks (though R_F is smaller than the

strong absorption radius $R_{1/2}$ (Ref. 37) by about 1 fm, as it should be). We have often $R_F - R_B \simeq 1$ fm, particularly for the cases with large X_{eff}, and we also found that the dominant contribution to the fusion cross section comes from a rather narrow region of about 1 fm width, between R_F and $R_D = R_F - 1.0$ fm. This means that all the fusion (and direct reactions) takes place outside the barrier. (We have shown this explicitly in Fig. 11 for an above barrier $E_{\text{c.m.}}$. This feature is even more noticeable as $E_{\text{c.m.}}$ is lowered, particularly below V_B.) In this sense, our picture of fusion is very different from that of BPM, where the fusion is assumed to take place after the ions pass through the barrier.

The fact that the fusion does not take place for $r \leq R_D$ is due to the fact that, inside R_D, the two-body $(A_1 + A_2)$ amplitude *de facto* vanishes, because of the absorptive nature of the optical potential. This means that, once one gets into the $r \leq R_D$ region, one should cease to think in terms of the simple $A_1 + A_2$ system. One must switch to a many-body type of description. The nucleons in A_1 and A_2 begin to attract each other, so as to form eventually a single (fused) nucleus.[38] This, we believe, is the physics which the optical potential, whose parameters are fixed so as to fit scattering and other DR data, tells us.

It will be interesting to compare the picture which we have presented just above with that of fission, particularly spontaneous fission (which may, to some extent, be considered to be a process inverse to sub-barrier fusion). As is well known, fission takes place if the system passes through a barrier, i.e., the saddle, which may be estimated to lie at a distance of about $1.0 \times (A_1^{1/3} + A_2^{1/3})$ fm. This saddle point is thus located inside R_B by 2 fm, say. An important fact to be presented here is that this barrier is not of a two-body, but of a many-body nature. No particular two-body channel $A_1 + A_2$ has yet been assigned in this barrier region. The separation of the system into $A_1 + A_2$ takes place only after the system passes through the barrier and reaches the scission point, which may correspond to the radius we called R_D. Thus our picture, which states that the fusion takes place even before the barrier is reached, is not inconsistent with the understanding of fission, in which the concept of barrier penetration is vital. Two quite different barriers are being talked about. The barrier talked about in the fusion description is a two-body barrier, while that of fission is a many-body barrier.

We have stressed above that we successfully fit the experimental σ_F, not only in the sub-barrier, but also in the above-barrier regions. In the latter, however, we have actually kept to the so-called region I, in which σ_F increases in proportion to $1/E_{\text{c.m.}}$. It is well known, however, that if $E_{\text{c.m.}}$ increases further, σ_F begins to saturate (region II) and even to decrease (region III). A natural question that is asked then is whether our method is applicable, even in these regions.

A preliminary study has been made to answer the above question, at least partially. It was done by taking the $^{16}O + ^{40}Ca$ system,[39] for which good information has been provided not only for σ_F, but also for the energy-dependent optical potential.

Since the details of this work will be published elsewhere,[40] we shall give here only a brief summary of the results obtained. In short, we were able to explain the transition from the region I to region II very naturally, which in particular means that the description was achieved by continuing to use the energy independent r_F. The key to this somewhat surprising result lies in the fact that the strength of the imaginary potential, in the energy dependent optical potential, suddenly increases[39] at just the $E_{\text{c.m.}}$ where the region I to region II transition takes place. This makes the $|\chi_{l_a}|^2$ factor in the integrand [in (3c) and (8b)] rather small for $r \leq R_F$. This fact prevented σ_F from increasing with increased $E_{\text{c.m.}}$.

The above result[40] presents us an interesting example to show, in addition to many other examples we have presented above, that it is indeed important to consider the DR (including elastic scattering) aspects, in understanding fusion properly, a point which we have stressed in the Introduction.

In the work done earlier, e.g., in BPM, information was also taken from the optical potential. Nevertheless, in most cases, the information that was taken was limited to only the real part of the optical potential. As our analyses given above have shown, and the related discussions have emphasized, however, it is the imaginary part, rather than the real part, of the optical potential that is playing the key role in our description of the fusion processes. After all, we are here treating heavy ions that are known to be very strongly absorptive. Correct information regarding their absorption would thus have to be taken into account properly.

We have not analyzed any data in the region III, in which σ_F is known to decrease with increasing $E_{\text{c.m.}}$. Thus, we are not in a position to make any definite statement about it, but may make the following remarks. One can certainly fit the data of decreasing σ_F, by keep reducing r_F. However, we do not consider it to be a correct way to follow. As is well known,[41] the critical angular momentum begins to play an important role at higher $E_{\text{c.m.}}$, preventing the information of compound systems with high spin values. This means that the correct method to use (within the framework of the present method) is to start introducing an angular momentum cutoff. This certainly gives rise to decreasing σ_F. The calculation of the contribution to fusion of the lower partial waves will, however, remain essentially unchanged from what we have done in the present paper.

ACKNOWLEDGMENTS

We are indebted to M. Beckerman and W. Henning for providing us with a few unpublished data. We are also grateful to D. M. Brink, B. A. Broglia, S. Landowne, R. G. Stockstad, and R. Vandenbosch for their enlightening discussions and encouragements. This work was supported in part by the U. S. Department of Energy. One of the authors (B.T.K.) acknowledges support from the Ministry of Education, Korea.

*Permanent address: Department of Physics, Sung Kyun Kwan University, Suwon, Korea.

[1]See, for instance, a review article by J. R. Birkelund and J. R. Huizenga, Annu. Rev. Nucl. Part. Sci. **33**, 265 (1983).

[2]L. C. Vaz, J. M. Alexander, and G. R. Satchler, Phys. Rep. **69**, 373 (1981).

[3]U. Jahnke, H. H. Rossner, D. Hilscher, and E. Holub, Phys. Rev. Lett. **48**, 17 (1982).

[4]H. Esbensen, Nucl. Phys. **A352**, 147 (1981).

[5]W. Reisdorf *et al.*, Phys. Rev. Lett. **49**, 1811 (1982).

[6]R. G. Stockstad *et al.*, Phys. Rev. Lett. **41**, 465 (1978); Phys. Rev. C **21**, 2427 (1980).

[7]R. G. Stockstad and E. E. Gross, Phys. Rev. C **23**, 281 (1981).

[8]G. M. Berkowitz *et al.*, Phys. Rev. C **28**, 667 (1983).

[9]M. Beckerman *et al.*, Phys. Rev. Lett. **45**, 1472 (1980); Phys. Rev. C **23**, 1581 (1981); **25**, 837 (1982).

[10]H. Sann *et al.*, Phys. Rev. Lett. **47**, 1248 (1981); R. Bock *et al.*, Nucl. Phys. **A388**, 334 (1982).

[11]R. A. Broglia, C. H. Dasso, S. Landowne, and A. Winther, Phys. Rev. C **27**, 2433 (1983).

[12]C. H. Dasso, S. Landowne, and A. Winther, Nucl. Phys. **A405**, 381 (1983).

[13]M. J. Rhodes Brown and P. Braun-Munzinger, Phys. Lett. **135B**, 19 (1984); M. J. Rhodes Brown and M. Prakash, Phys. Rev. Lett. **53**, 333 (1984).

[14]S. Landowne and S. C. Pieper, Phys. Rev. C **29**, 1352 (1984).

[15]W. J. Swiatecki, Nucl. Phys. **A376**, 279 (1982).

[16]C. Grègoire, C. Ngo, and B. Remand, Nucl. Phys. **A383**, 392 (1982).

[17]T. Udagawa and T. Tamura, Phys. Rev. C **29**, 1922 (1984).

[18]B. T. Kim, T. Udagawa, and T. Tamura, in *Proceedings of the International Conference on Fusion Reactions below the Coulomb Barrier, MIT, Cambridge, Mass., 1984,* edited by S. G. Steadman (Springer, Berlin, 1984), p. 142; T. Tamura, T. Udagawa, and B. T. Kim, J. Phys. Soc. Jpn. Suppl. (to be published).

[19]H. Feshbach, Ann. Phys. (N.Y.) **19**, 287 (1967).

[20]K. Kawai, A. K. Kerman, and K. McVoy, Ann. Phys. (N.Y.) **25**, 156 (1973).

[21]We use here the notation R_F, instead of R_{cr}, which we used earlier in Ref. 17. We want to avoid a possible mixing up of our R_F with the *critical distance,* which has been used in the BPM-type works, and could possibly be denoted by R_{cr}. For R_{cr}, see, e.g., J. Galin *et al.*, Phys. Rev. C **9**, 1018 (1974); D. Glass and U. Mosel, *ibid.* **10**, 2620 (1974).

[22]T. Tamura, Rev. Mod. Phys. **37**, 679 (1965).

[23]W. R. Coker, T. Udagawa, and H. H. Wolter, Phys. Rev. C **7**, 1154 (1973).

[24]T. Udagawa and T. Tamura, Phys. Rev. C **24**, 1348 (1981); T. Udagawa, Lecture notes given at RCNP-KIKUCHI Summer School on Nuclear Physics, Kyoto, Japan, 1983, edited by H. Katayama and H. Ogata (Osaka University, Osaka, Japan, 1983), p. 33.

[25]F. Videbaek *et al.*, Phys. Rev. C **15**, 954 (1977).

[26]H. C. Britt *et al.*, Phys. Rev. C **13**, 1484 (1976).

[27]H. Doubre *et al.*, Phys. Rev. C **15**, 693 (1977).

[28]W. Henning, in *Proceedings, of the International Conference on Fusion Reactions below the Coulomb Barrier, MIT, Cambridge, Mass., 1984,* edited by S. G. Steadman (Springer, Berlin, 1984), p. 150; W. S. Freeman *et al.*, Phys. Rev. Lett. **50**, 1563 (1983).

[29]K. A. Erb *et al.* (unpublished), quoted by F. Plasil, Nucl. Phys. **A400**, 417c (1983).

[30]J. Barreto, G. Auger, M. Langevin, and E. Plagnol, Phys. Rev. C **27**, 1335 (1983); H. A. Aljumair *et al.*, *ibid.* **30**, 1223 (1984).

[31]M. Beckerman *et al.*, in *Proceedings of the International Conference on Fusion Reactions below the Coulomb Barrier, MIT, Cambridge, Mass., 1984,* edited by S. G. Steadman (Springer, Berlin, 1984), p. 1.

[32]M. Beckerman, J. Wiggins, H. Aljuwair, and M. K. Salomaa, Phys. Rev. C **29**, 1938 (1984).

[33]R. Vandenbosch *et al.*, Phys. Rev. **28**, 1161 (1983).

[34]K. E. Rehm *et al.*, Phys. Rev. Lett. **51**, 1426 (1983).

[35]B. T. Kim, Phys. Lett. **80B**, 353 (1979).

[36]In this regard we may remark that C. Signorini *et al.*, J. Phys. Soc. Jpn. Suppl. (to be published), presented cases in which the sub-barrier σ_F are not necessarily very large, even when channels with positive Q values are involved. In these cases, however, $|Q|$ is relatively small, being of the order of 1 MeV.

[37]G. R. Satchlar, in *Proceedings of the International Conference on Reactions between Complex Nuclei, Nashville, 1974,* edited by R. L. Robinson *et al.* (North-Holland, Amsterdam, 1974), Vol. 2, p. 171.

[38]K. Goecke and P. G. Reinhard, Ann. Phys. (N.Y.) **114**, 328 (1978); J. W. Negele, Rev. Mod. Phys. **54**, 913 (1982).

[39]S. E. Vigdor *et al.*, Phys. Rev. C **20**, 2147 (1979).

[40]T. Udagawa, S. W. Hong, and T. Tamura (unpublished).

[41]S. F. Cohen, F. Plasil, and W. J. Swiatecki, Ann. Phys. (N.Y.) **82**, 557 (1974); J. Wilczynski, Nucl. Phys. **A216**, 386 (1973); M. Ohta, K. Hatogai, S. Okai, and Y. Abe, Phys. Rev. C **29**, 1948 (1984).